Itaconate Inhibits TET DNA Dioxygenases to Dampen Inflammatory Responses

Dan Ye (yedan@fudan.edu.cn)
Fudan University
Leilei Chen
Fudan University, Shanghai, China
Carmen Morcelle
Fudan University, Shanghai, China
Zhouli Cheng
Fudan University, Shanghai, China
Xiufei Chen
Institutes of Biomedical Sciences, Shanghai Medical College of Fudan University
Yanping Xu
Tongji University
Yajing Gao
Institutes of Biomedical Sciences, Shanghai Medical College of Fudan University
Jun-Bin Song
Key Laboratory of Medical Epigenetics and Metabolism, and Molecular and Cell Biology Lab, Institutes of Biomedical Sciences, Shanghai Medical College, Fudan University
Zhijun Li
University of North Carolina
Matthew Smith
Lineberger Comprehensive Cancer Center, University of North Carolina at Chapel Hill
Miao Shi
Life Sciences Institute and Stem Cell Institute, Zhejiang University, Hangzhou
Yezhang Zhu
Zhejiang University
Neng Zhou
Key Laboratory of Pediatric Hematology and Oncology Ministry of Health and Pediatric Translational Medicine Institute, Shanghai Children's Medical Center, Shanghai Jiao Tong University of Med
Meng Cheng
Lineberger Comprehensive Cancer Center, University of North Carolina at Chapel Hill
Chenxi He
Kwei-Yan Liu
Kaohsiung Medical University

Guoping Lu
Department of Critical Care Medicine, Children's Hospital of Fudan University
Lei Zhang
Fudan University
Cheng Zhang
https://orcid.org/0000-0002-9218-5019
Jinye Zhang
https://orcid.org/0000-0002-8947-2607
Yiping Sun
Shanghai Medical College of Fudan University
Tuan Qi
Key Laboratory of Growth Regulation and Translational Research of Zhejiang Province, School of Life Sciences, Westlake University
Yingying Lyu
Department of Neurosurgery, Huashan Hospital, Fudan University, Shanghai 200040, China
Zhi-Zhong Ren
Lineberger Comprehensive Cancer Center, University of North Carolina at Chapel Hill
Xian-Ming Tan
Lineberger Comprehensive Cancer Center, University of North Carolina at Chapel Hill
Fei Lan
Fudan University
Ying Liu
Department of Pathology, School of Basic Medical Sciences, Shanghai Medical College, Fudan University
Hui Yang
Department of Neurosurgery, Huashan Hospital, Fudan University
Caiwen Duan
Key Laboratory of Pediatric Hematology and Oncology Ministry of Health and Pediatric Translational Medicine Institute, Shanghai Children’s Medical Center, Shanghai Jiao Tong University of Med
Xing Chang
Key Laboratory of Growth Regulation and Translational Research of Zhejiang Province, School of Life Sciences, Westlake University, Hangzhou, China
Yufeng Zhou
Fudan University https://orcid.org/0000-0002-6050-4951
Li Shen
Zhejiang University https://orcid.org/0000-0002-5696-2191
Albert Baldwin
University of North Carolina at Chapel Hill
Kun-Liang Guan

Department of Pharmacology and Moores Cancer Center, University of California San Diego

Yue Xiong

Lineberger Comprehensive Cancer Center, Department of Biochemistry and Biophysics, University of North Carolina at Chapel Hill

---

Article

Keywords: inflammatory response, IRG1, immune response

Posted Date: September 23rd, 2021

DOI: https://doi.org/10.21203/rs.3.rs-900207/v1

Version of Record: A version of this preprint was published at Nature Cell Biology on March 7th, 2022. See the published version at https://doi.org/10.1038/s41556-022-00853-8.

Abstract

The immune-response gene 1 (IRG1) plays a key role in anti-pathogen defense, as deletion of Irg1 **in mice causes severe defects in response to bacterial and viral infection, and decreased survival**[1,2]. IRG1 **transcription is rapidly induced by pathogen infection and inflammatory conditions primarily in cells of myeloid lineage**[3]. **IRG1 encodes a mitochondrial metabolic enzyme, aconitate decarboxylase 1 (ACOD1), that catalyzes the decarboxylation of cis-aconitate to produce the anti-inflammatory metabolite itaconic acid (ITA)**[4]. **Several molecular processes are affected by ITA, including succinate dehydrogenase (SDH) inhibition**[5], **resulting in succinate accumulation and metabolic reprogramming**[6,7], **and alkylation of protein cysteine residues, inducing the electrophilic stress response mediated by NRF2 and IκBζ**[8,9] **and impairing aerobic glycolysis**[10]. **However, the mechanisms by which ITA exerts its profound anti-inflammatory effect still remains to be fully elucidated. Here, we show that ITA is a potent inhibitor of the TET family DNA dioxygenases, which catalyze the conversion of 5-methylcytosine (5mC) to 5-hydroxymethylcytosine (5hmC) during the process of active DNA demethylation. ITA binds to the same site of α-ketoglutarate (α-KG) in TET2, inhibiting its catalytic activity. Lipopolysaccharides (LPS) treatment, which induces Irg1 expression and ITA accumulation, inhibits Tet activity in macrophages. Transcriptome analysis reveals TET2 is a major target of ITA in suppressing LPS-induced genes, including those regulated by NF-κB and STAT signaling pathways.** In vivo, **ITA decreases 5hmC, reduces LPS-induced acute pulmonary edema and lung and liver injury, and protects mice against lethal endotoxaemia in a manner that is dependent on the catalytic activity of Tet2. Our study thus identifies ITA as an immune modulatory metabolite that selectively inhibits TET enzymes to dampen the inflammatory response.**

Main

Deletion of the *Irg1* gene or treatment with cell permeable ITA alters the transcriptional signature in response to LPS[2]. We speculated that ITA may impact epigenetics to influence gene expression, and therefore, we determined the effect of Irg1 expression and ITA accumulation on global histone and DNA de/methylation in transfected HEK293T cells (Extended Data Fig. 1a). We found that ectopic expression of either wild-type or catalytic inactive mutant Irg1 had little effect on mono-, di-, and trimethylation of all five histone H3 lysine residues (Extended Data Fig. 1b, 1c). In contrast, expression of wild-type Irg1, but not the catalytic inactive mutant, dramatically reduced Tet2-mediated global 5hmC in cells (Fig. 1a and Extended Data Fig. 1d-e). Like α-KG, which is a crucial co-substrate for the activity of TET2, ITA is also a dicarboxylic acid containing a 4- or 5-carboxylate that, in the case of α-KG, forms hydrogen and ionic bonds with H1416, R1896, and S1898 in TET2[11]. Of note, α-KG binds to Fe(II) in a bidentate manner via its C-1 carboxylate and C-2 keto groups, which are lacking in ITA. This raises the possibility that ITA may act as an α-KG antagonist to competitively inhibit TET and other α-KG/Fe(II)-dependent dioxygenases, similar to previously identified oncometabolites, D-2-HG, succinate, and fumarate. Molecular modeling suggests that ITA, like the other α-KG antagonists, can interact with amino acid residues within the active site of TET2 (Extended Data Fig. 2a).

In vitro biochemical assays revealed that ITA effectively blocked the activity of purified mouse TET2 Cys-rich and DSBH domains ($mTET2^{CD}$), as determined by the conversion from 5mC to 5hmC (Fig. 1b and Extended Data Fig. 2b). Using another *in vitro* enzymatic assay based on immobilized substrate DNA and fluorescence detection of 5hmC (Extended Data Fig. 2c), we found ITA inhibited the catalytic activity of $mTET2^{CD}$ with a half maximal inhibitory concentration (IC_{50}) of 171 μM (Fig. 1c), similar to that of L-2-HG (115 μM) and considerably more potent than D-2-HG (1,057 μM), succinate (> 5mM) and fumarate (> 5 mM). Similar results were obtained when using a commercial TET activity assay kit (Extended Data Fig. 2d). The inhibition of $mTET2^{CD}$ activity by ITA or L-2-HG was overcome dose-dependently by excess α-KG (Fig. 1d). Furthermore, saturation transfer difference (STD) NMR spectroscopy demonstrated that ITA, but not glutamine as a negative control metabolite, bound directly to recombinant human $TET2^{CD}$ and that ITA-$TET2^{CD}$ binding was blocked by α-KG (Fig. 1e). Mutation of either R1896 or S1898 in TET2 reduced its 5hmC-producing activity. These mutations, associated with weakened binding of α-KG in TET2 (Extended Data Fig. 2e, 2f), were found to also abolish the binding of ITA (Fig. 1f). Together, these results demonstrate that ITA binds directly to TET2 in a manner similar to α-KG and potently inhibits TET activity.

To determine whether ITA inhibits the TET family enzymes in cells, we treated RAW264.7 mouse macrophages with octyl-ITA (OI) or unmodified ITA and confirmed rapid (< 30 seconds) intracellular accumulation of ITA in a dose-dependent manner and inhibition of SDH by ITA, as seen by the accumulation of succinate (Extended Data Fig. 3a, 3b). OI, like cell-permeable Octyl-L-2HG, accumulated in HEK293T cells overexpressing $mTET2^{CD}$ and dose-dependently reduced 5hmC (Extended Data Fig. 3c, 4a). This reduction was reversed by the addition of increasing amount of cell-permeable dimethyl-α-KG (Extended Data Fig. 4b). Likewise, in HEK293T cells overexpressing TET3, exogenously added OI or ITA led to intracellular accumulation of ITA and decreased global 5hmC (Extended Data Fig. 4c, 4d ,4e and 4f). Unlike L-2-HG, which also inhibits JmjC-domain histone lysine demethylases (KDMs)[12, 13], and in accord with Irg1 overexpression (Extended Data Fig. 1c), addition of OI had no detectable effect on global histone methylation (Extended Data Fig. 4g), supporting a selective inhibition of ITA towards TET enzymes over KDMs.

Given that the anti-inflammatory metabolite ITA is accumulated primarily in cells of myeloid lineage[3], we treated *Tet2*$^{+/+}$ and *Tet2*$^{-/-}$ bone marrow-derived macrophages (BMDMs) with either OI or ITA. In these cells, intracellular accumulation of ITA was observed along with a reduction in genomic 5hmC in an ITA-dose-dependent manner in *Tet2*$^{+/+}$ BMDMs (Extended Data Fig. 5a and 5b). Global mapping of 5hmC via DNA immunoprecipitation coupled with high-throughput sequencing (hMeDIP-seq) showed that OI treatment decreased 5hmC at both promoters and intragenic regions in *Tet2*$^{+/+}$ BMDMs (Extended Data Fig. 5c). Quantitative LC–MS/MS analysis further confirmed that exogenously added OI or ITA reduced global 5hmC by as much as 95% in *Tet2*$^{+/+}$ BMDMs but had little effect in *Tet2*$^{-/-}$ cells, in which basal levels of 5hmC were already reduced by ~92% (Fig. 2a). These findings thus suggest that Tet2 is the key TET enzyme controlling 5hmC production in macrophages and can be nearly completely inhibited by exogenous ITA.

Consistent with previous studies[3, 4], LPS treatment rapidly induced *Irg1* mRNA within 30 min in RAW264.7 macrophages, followed by protein accumulation within 2 hours (Extended Data Fig. 6a, 6b). As a result, endogenous ITA rapidly accumulated to millimolar levels between 2 to 4 hours after LPS stimulation, and reached as high as 3.75 mM before starting to decline (Extended Data Fig. 6d). This accumulation was completely abolished by deletion of the *Irg1* gene (Extended Data Fig. 6c, 6d). LPS treatment also induced the accumulation of succinate but had no significant effect on fumarate or 2-HG levels (Extended Data Fig. 6e). As previously noted[14, 15], α-KG levels were also affected, decreasing from ~0.4 mM in untreated macrophages to ~0.2 mM at 4 hours after LPS stimulation (Extended Data Fig. 6e).

In macrophages examined, *Tet1* mRNA expression was extremely low, while the mRNA expression of *Tet2* and *Tet3* was up-regulated and down-regulated by LPS treatment, respectively (Extended Data Fig. 7a). Interestingly, global 5hmC was reduced by LPS stimulation in *Irg1*-WT RAW264.7 cells but stayed relatively higher in *Irg1*-KO cells, as determined by LC-MS/MS (Fig. 2b), immunofluorescence staining (Extended Data Fig. 7b), and FACS analysis (Extended Data Fig. 7c). Treatment of LPS-stimulated *Irg1*-KO RAW264.7 cells with 3-nitropropionic acid (3-NPA), a specific SDH inhibitor, led to intracellular accumulation of succinate to as high as 1.5 mM, but had little effect on global 5hmC (Extended Data Fig. 7d). This result argues against the model that succinate, which is accumulated by ITA-mediated SDH inhibition and itself an inhibitor of Tet enzymes[16], is responsible for the LPS-induced TET inhibition. Moreover, the addition of dimethyl-α-KG restored 5hmC in LPS-treated RAW264.7 cells (Extended Data Fig. 7e), further supporting that α-KG and ITA competitively interact with TET enzymes. In line with cell treatment with exogenous ITA (Extended Data Fig. 4g), LPS induction of ITA had no effect on global histone methylation in RAW264.7 cells (Extended Data Fig. 7f).

In accord with Tet2 transcription, its protein expression was induced by LPS in BMDMs and peritoneal macrophages (PMs) (Extended Data Fig. 8a-b). Deletion of *Irg1* did not affect Tet2 induction by LPS, but increased 5hmC by 1.9-folds compared to LPS-treated *Irg1*$^{+/+}$ BMDMs (Fig. 2c). In PMs, deletion of *Irg1* increased both basal and post-LPS levels of 5hmC, with the latter being 2.5-fold higher in *Irg1*$^{-/-}$ than *Irg1*$^{+/+}$ PMs (Fig. 2d). Furthermore, 5hmC mapping demonstrated that deletion of *Irg1* increased 5hmC at promoter and intragenic regions in LPS-stimulated BMDMs (Fig. 2e). These results thus suggest that ITA, which is produced by IRG1 during the inflammatory response, selectively inhibits TET enzymes.

Several mechanisms have been proposed for the anti-inflammatory function of ITA[17]. For instance, ITA may directly inhibit SDH[5], resulting in succinate accumulation and metabolic reprogramming[6, 7]; how succinate accumulation contributes to the anti-inflammatory function of ITA remains unclear. ITA is also known to act as an electrophile in Michael reactions to alkylate cysteine residues in proteins, including KEAP which targets NRF2, and to induce electrophilic stress through activating NRF2- or IκBζ-mediated pathways[8, 9]. Nonetheless, ITA can also influence the expression of genes, such as *IκBζ, IL-6, TNF* and *ATF3*, independently of NRF2[9], and the precise mechanism by which ITA affects gene expression remains largely unknown. To investigate the role of TET enzymes as effectors of ITA, we compared the transcriptome changes caused by either OI treatment, which caused inhibition of Tet2 catalytic activity, or

Tet2 deletion (*Tet2*-KO) in LPS-stimulated RAW264.7 cells (Extended Data Fig. 9a). At least 2-fold up- or down-regulation was observed in 3,734 genes when treating *Tet2*-WT cells with OI, and in 3,717 genes upon *Tet2* deletion (Fig. 3a). Considering that the catalytic function of TET enzymes is typically associated with gene activation, we thus focused on the genes which were down-regulated by OI upon LPS stimulation. While OI treatment led to 1,846 down-regulated genes in *Tet2*-WT cells, it down-regulated only 807 genes in *Tet2*-KO cells. Only 493 (27%) out the 1,846 genes down-regulated by OI treatment in *Tet2*-WT cells were also down-regulated by OI in *Tet2*-KO cells (Extended Data Fig. 9b), indicating that in absence of Tet2, a large proportion (73%) of genes downregulated by ITA are no longer affected. We further focused on LPS-inducible genes in macrophages. Of 1,846 genes that were down-regulated by OI treatment in *Tet2*-WT cells, 712 were induced by LPS by at least 2-folds (Extended Data Fig. 9c). Of these 712 genes, 509 (71.5% of the total) were also down-regulated by *Tet2* deletion in LPS-stimulated cells (Fig. 3b), whereas only 135 (19.0% of the total) were down-regulated by OI treatment in *Tet2*-KO cells (Extended Data Fig. 9d). These results thus indicate that a significant fraction of LPS-induced genes is commonly regulated by ITA and Tet2. Many of these genes are involved in the innate immune and inflammatory responses, including signaling pathways mediated by cytokines, such as TNF, Toll-like receptor, and NF-κB (Fig. 3b). K-mean clustering of the 712 LPS-induced and OI-inhibited genes showed similar expression patterns in macrophages between OI treatment and *Tet2*-KO upon LPS stimulation (Fig. 3c). Together, these data support the notion that ITA acts largely through Tet2 to inhibit the expression of LPS inducible genes in macrophages.

TET2 has both catalytic dependent and independent functions[18]. To gain more insight into ITA influencing gene expression through inhibiting the catalytic activity of TET2, we generated *Tet2*^{H1795R} knock-in (KI) mutant mice. H1795 in mouse Tet2 is equivalent to human TET2 H1881, which is recurrently mutated in human acute myeloid leukemia and is essential for TET2 catalytic activity[19]. We confirmed the catalytic-defective mutation H1795R by genotyping and 5hmC dot-blot assay (Extended Data Fig. 9e, 9f). We then isolated *Tet2*$^{+/+}$ and *Tet2*^{H1795R} (*Tet2*-KI) BMDMs and treated them with LPS either alone or together with OI, followed by gene expression profiling analysis. Of 1,463 genes that were induced by LPS and down-regulated by OI treatment, 607 (41.5%) were down-regulated by *Tet2*-KI (Extended Data Fig. 9g). KEGG signaling pathways analysis of these 607 genes revealed that, similarly to our findings in *Tet2*-KO cells, they were also enriched for genes involved in innate immune and inflammatory responses (Extended Data Fig. 9g), including four pathways dually impaired by both OI treatment and *Tet2* deletion in RAW264.7 cells.

Many genes from the four above-mentioned pathways encode chemokines, interleukins, and their receptors (Fig. 3d). Among these genes, *Nfkbiz* encodes IκBζ, an atypical IκB member and a transcriptional regulator of selective NF-κB target genes. IκBζ regulates IL-6 production in macrophages and other cell types[20], as well as IFN-γ production in NK cells[21], and it is involved in Th17 development[22], psoriasis[23], and cellular senescence[24]. Three (T_H1)-type chemokines, Cxcl9, Cxcl10, and Cxcl11, are transcriptionally activated by STAT1-recruited TET2 following interferon treatment[25] and attract effector T cells during the inflammatory response[26]. To provide further evidence supporting TET2 as the major

target of ITA, we examined the regulation of selected genes by Irg1/ITA and Tet2 in detail. Our data demonstrated that the effect of exogenous ITA on suppressing LPS-induced chemokine and cytokine genes was completely abolished by *Tet2* deletion (Fig. 3e and Extended Data Fig. 10a). To eliminate interference factors from endogenous ITA, we found that shortly after LPS stimulation before endogenous ITA started accumulating, addition of OI still hindered LPS-induced mRNA expression of *Nfkbiz, Il-6,* and *Cxcl9/10/11,* in *Tet2*-WT macrophages, mimicking the effect of *Tet2* deletion (Extended Data Fig. 10b). In contrast, LPS-induced mRNA expression of chemokines and cytokines was further increased by *Irg1*-deletion in macrophages (Fig. 3f).

Members of the NF-κB transcription factor family play a critical role in innate immunity in response to pathogen infections, tissue injury, and tumor inflammation[27]. Among 16 members of NF-κB, IκB and IKK families, *Nfkbiz* was the only one whose induction by LPS was hindered by Tet2 inactivation (by either OI treatment or *Tet2*-KI) or *Tet2* deletion (Extended Data Fig. 11a, 11b, 11c). OI treatment failed to affect *Nfkbiz* mRNA expression in LPS-stimulated *Tet2*-KO cells (Extended Data Fig. 11d), and treatment with dimethyl-α-KG was able to further increase *Nfkbiz* mRNA in LPS-stimulated *Tet2*-WT but not *Tet2*-KO cells (Extended Data Fig. 11e, 11f). In accord, western blotting analysis confirmed the effects of ITA and α-KG on inhibiting and stimulating LPS-induced IκBζ protein, respectively, in a Tet2-dependent manner (Extended Data Fig. 11g, 11h). Together, these results support TET2 as the major target of ITA function in suppressing LPS-induced genes, including those regulated by both NF-κB and STAT1 immune signaling pathways.

TET2 is known to be recruited to DNA by multiple sequence-specific transcription factors (TFs), including WT1[19, 28], STAT3[29], CXXC5[30], and STAT1[31]. In searching for TFs that might recruit TET2 to regulate LPS-induction of *Nfkbiz*, we found that LPS stimulated Tet2 binding with NF-κB p65/RelA in RAW264.7 cells (Extended Data Fig. 12a, 12b). The proximal promoter region of mouse *Nfkbiz* gene contains three putative canonical κB sites and two of them, κB1 and κB2, are conserved in the human *Nfkbiz* promoter[32] (Extended Data Fig. 12c). Systematic investigation of TF binding in resting or activated macrophages has previously identified RelA bindings at the *Nfkbiz* promoter[33]. We confirmed the binding of RelA to the *Nfkbiz* promoter and found that it was stimulated by LPS but abolished by *RelA* knockdown (Extended Data Fig. 12d). Tet2 bound to the *Nfkbiz* promoter (Extended Data Fig. 12e), and this binding was stimulated by LPS in a manner dependent on RelA (Extended Data Fig. 12f). In accord with Tet2 occupancy, 5hmC in the *Nfkbiz* promoter was low in unstimulated macrophages, while was increased by 4.3-folds after LPS stimulation, and this increase was abolished by *RelA* knockdown (Extended Data Fig. 12g). Along with lower levels of 5hmC at the *Nfkbiz* promoter, *RelA* knockdown led to decreased *Nfkbiz* mRNA levels in RAW264.7 cells during the LPS response, as observed upon TET2 loss (Extended Data Fig. 12h, 12j). In contrast, *Nfkbiz* mRNA was up-regulated by *Irg1*-KO in LPS-stimulated macrophages (Extended Data Fig. 12h), which was associated with higher 5hmC in the *Nfkbiz* proximal promoter region (Extended Data Fig. 12i). Similar to *Nfkbiz*, the expression of multiple Tet2-dependent cytokine and chemokine genes was also inhibited by *RelA* knockdown in LPS-stimulated macrophages (Extended Data

Fig. 12j). Taken together, these results suggest that, in response to LPS stimulation, p65 NF-κB/RelA recruits Tet2 to induce DNA demethylation and gene expression.

To further investigate the role of ITA-mediated TET2 inhibition *in vivo*, intraperitoneal injection of LPS was conducted to induce inflammation in mice. We found that at four hours post LPS challenge, ITA in *Irg1*$^{+/+}$ peritoneal leukocytes was increased by 13.5-folds (from ~23.5 μM to 316.7 μM) (Extended Data Fig. 13a, 13b). Basal 5hmC was similar between *Irg1*$^{-/-}$ and *Irg1*$^{+/+}$ leukocytes, while it was significantly higher in LPS-challenged *Irg1*$^{-/-}$ leukocytes than *Irg1*$^{+/+}$ cells (Fig. 4a). Quantitative LC-MS/MS analysis confirmed that genomic 5hmC was 2.5-fold higher in *Irg1*$^{-/-}$ leukocytes than *Irg1*$^{+/+}$ cells at four hours after LPS injection (Fig. 4b). ChIP-qPCR analysis demonstrated that 5hmC at the *Nfkbiz* promoter was stimulated by LPS in WT, but not *Tet2*$^{-/-}$ leukocytes and, importantly, deletion of *Irg1* further increased 5hmC at *Nfkbiz* promoter by 1.8-fold as compared to WT cells after LPS challenge (Fig. 4c). In LPS-stimulated leukocytes of different genotypes, 5hmC levels at the *Nfkbiz* promoter closely correlated to its mRNA levels, which were the highest in LPS-challenged *Irg1*$^{-/-}$ leukocytes followed by WT and then *Tet2*$^{-/-}$ cells (Fig. 4d). In addition, we also extended this finding to other target genes of NF-κB-TET2 and STAT1-TET2 axes, including *Cxcl9, Cxcl10, Cxcl11, Il6, Il-12a*, and *Il-15* (Fig. 4d).

Next, we employed a mouse model of LPS-induced sepsis and found that in line with our findings in isolated leukocytes (Fig. 4d), serum Il-6 was higher in LPS-challenged *Irg1*$^{-/-}$ mice than *Irg1*$^{+/+}$ controls (Extended Data Fig. 13c). *Irg1*$^{-/-}$ mice were more susceptible to LPS-induced acute lung injury and had higher mortality (Extended Data Fig. 13d, 13e, 13f), confirming the role of Irg1/ITA in dampening LPS-induced inflammatory response. Conversely, intraperitoneal injection of ITA led to reduced 5hmC by as much as 36% in peritoneal leukocytes, while 5mC was unaffected (Extended Data Fig. 14a). ITA treatment was able to attenuate LPS-induced pulmonary edema (wet-to-dry ratio, W/D; Extended Data Fig. 14b) as well as acute lung injury (Extended Data Fig. 14c, 14d), and protected mice against lethal endotoxaemia (Extended Data Fig. 14e). These anti-inflammatory and protective effects of ITA were not observed in *Tet2*$^{-/-}$ mice (Extended Data Fig. 14b, 14c, 14d, 14f).

To further strengthen the functional significance of the Irg1/ITA/Tet2 axis, chimeric mice were developed by transplanting bone marrow cells from catalytically inactive *Tet2*^{HxD} knock-in (KI) mutant or WT mice (Extended Data Fig. 14g). The *Tet2*^{HxD} KI mutant mice contain H1295Y and D1297A double substitution mutations in mouse Tet2, which are equivalent to human TET2 H1382 and H1384, respectively[34], and disrupt the binding with the essential cofactor Fe^{2+}. Reconstitution of hemapotoiesis with *Tet2*^{HxD} bone marrow led to ~50% reduction in global 5hmC in transplanted animals (Extended Data Fig. 14h, 14i). Compared with WT chimeric mice, *Tet2*^{HxD} chimeric mice had dampened LPS-induced inflammatory responses, including lower serum levels of pro-inflammatory cytokines and chemokines such as Il-6, Tnf-a, Cxcl9 (Fig. 4e), reduced serum activities of ALT and AST (liver damage markers; Fig. 4f), less severe pulmonary edema (Fig. 4g) and lung injury (Fig. 4h, 4i), and prolonged survival (Fig. 4j). Importantly, these molecular, tissue and animal changes caused by the catalytic inactivation of Tet2 were all recapitulated in ITA-pretreated WT chimeric mice upon LPS challenge (Fig. 4e-4j). These results thus provide direct *in*

vivo evidence to support that TET2 is a major functional target of ITA and that the Irg1/ITA/Tet2 axis plays a key physiological role in immune modulation.

Four metabolites, D-2HG, succinate, fumarate, and L-2HG, have previously been reported to inhibit TET and other α-KG/Fe(II)-dependent dioxygenases such as histone demethylase KDMs. Among these four metabolites, D-2HG accumulates in cancer cells with mutated isocitrate dehydrogenases (IDH1/2), while L-2HG is produced by the promiscuous activity of either lactate dehydrogenase (LDH) or malate dehydrogenase (MDH) in cells under acidic or hypoxic conditions[35]. Succinate and fumarate can accumulate as a result of loss-of-function mutations in cancer cells affecting SDH and fumarate dehydrogenase (FH), respectively, as well as under certain conditions such as glutamine replenishment of the TCA cycle[36, 37]. In contrast to these metabolites, ITA is the primary reaction product of the metabolic enzyme IRG1, whose levels remains virtually undetectable in the absence of stimuli and are boosted in cells of myeloid lineage during the inflammatory response. Unlike above-mentioned four metabolites which inhibit both TET and KDM enzymes involved in epigenetic regulation, ITA is the first physiological metabolite that selectively inhibits TET enzymes.

Our results presented here connect the function of Irg1/ITA and Tet2 during inflammatory response. Mutations in TET2 lead to clonal hematopoiesis, altered response to immunotherapy, atherosclerosis, and hematopoietic malignancy[38-40]. Separately, genetic studies in mice have demonstrated a critical function of *Irg1* in inflammatory response to wide range of pathogens, such as *M. tuberculosis* [2], Zika virus [1], *Salmonella*[41] and LPS (Fig 4). Not only does our study demonstrate that TET2 is inhibited by ITA, but also that TET2 is a major functional target of ITA. Furthermore, this study uncovers three new regulatory mechanisms linked to the inflammatory response, that is, the inhibition of TET2 by the anti-inflammatory metabolite ITA, the functional interaction between TET2 and a key inflammatory regulator NF-κB, and the transcriptional activation of a key driver in inflammation, IκBζ, by TET2-mediated DNA demethylation and subsequent downregulation by ITA inhibition of TET2. Together, these findings establish a novel Irg1/ITA-Tet2-NF-κB-IκBζ axis that mediates inflammatory response.

TET2 is recruited by WT1[19, 28], STAT3[29], CXXC5[30], STAT1[31], and NF-κB (Fig. 4) to regulate immune cell differentiation, homeostasis and function. STAT and NF-κB mediate two principal signaling pathways during the inflammatory response in different types of immune cells, including macrophages. In this study, we show that Irg1/ITA inhibits Tet2 to dampen LPS-induced expression of both the NF-κB-TET2 and STAT1-TET2 target genes in macrophages, while deletion of *Irg1* leads to transcriptional activation of these genes (Fig. 3 and Fig. 4). The inhibition of NF-κB-Tet2 and STAT1-Tet2 by ITA provides a molecular basis of how ITA can exert an inhibitory effect on many proinflammatory genes in both STAT and NF-κB signaling pathways (Extended Data Fig. 15). Such broad function of ITA is consistent with the induction of IRG1 by diverse pathogens such as *Mycobacterium*[2, 42], *Salmonella* [41], influenza A virus [43], West Nile virus [44], Zika virus [1], Marek disease virus [45] and *T.gondii* [46], as well as induction in human PBMCs of sepsis patients [47]. In addition to viral and bacterial infection, IRG1 is also induced in *Zebrafish* epidermal cells during cutaneous inflammation[48], by particulate matter air pollution [49], during peritoneal

tumorigenesis[50], and embryonic implantation[51]. The results presented here support the biological relevance of TET inhibition by ITA in broad physiological and pathological processes and provide new insights into the regulation of these processes.

Methods

Animals and study approval

Tet2$^{-/-}$ mice (JAX stock #023359) and *Irg1*$^{-/-}$ mice (JAX stock #029340) were purchased from the Jackson Laboratory. Animals were backcrossed for more than 7 generations onto the C57BL/6J background and were maintained at Shanghai Research Center for Model Organisms. Animals were given unrestricted access to a standard diet and tap water. Animal experiments were performed at Fudan Animal Center in accordance with animal welfare guidelines, and the procedures were approved by the Ethics Committee of the Institutes of Biomedical Sciences (IBS), Fudan University.

Tet2^{H1795R} KI mutant mice were generated by gene targeting in ES cells from 129P2/Ola background strain microinjected into strain C57BL/6 blastocysts, and successful point mutant insertion was confirmed by PCR and DNA sequencing by the UNC Animal Models Core (AMC). Likewise, the AMC generated knockout mice by direct pronuclear injection of *Tet2* mRNA and sgRNAs targeting genes of interest in embryos. Successful knockout was confirmed by Southern, PCR and DNA sequence. A single founder was identified with mutations in genes and mated to C57BL/6J females. The remaining conditional and conventional knockout mice were generated by gene targeting in ES cells from C57BL/6 background strain microinjected into albino-C57BL/6 blastocysts. Successful knockout was confirmed by Southern, PCR and DNA sequence. The animal experiments were approved by the IACUC at UNC–Chapel Hill.

Tet2^{HxD} KI mutant mice on C57BL/6J background were constructed by using CRISPR/Cas9 system and were kindly provided by Dr. Jiayu Chen and Dr. Shaorong Gao (School of Life Sciences and Technology, Tongji University, Shanghai). *Tet2*^{HxD} KI and sex-matched wild-type mice were used as donor for bone marrow transplantation (BMT): In brief, C57BL/6 J mice (male, 8-10 weeks old) underwent total body irradiation with a total of 7.5 Gy from a cesium source, and the lethally irradiated recipients were transplanted with 2x10^6 whole bone marrow cells of donors by tail vein injection. The transplanted animals were maintained on antibiotic water in pathogen-free facilities at Shanghai Children's Medical Center. The rate of chimerism in each transplanted animal was verified by PCR sequencing upon sacrifice. At 6 weeks after BMT, antibiotic water was withdrawed for 3 days, and the transplanted animals were subjected to a model of LPS-induced sepsis as decribed below. The animal experiments were approved and supervised by the Animal Research Committee (ARC) of Shanghai Jiao Tong University of Medicine with proper ethical regulations.

Cell culture

RAW264.7 cells (ATCC® TIB-71™, passage 25) and HEK293T cells (ATCC® CRL-3216™) were acquired from UNC Lineberger Tissue Culture Facility and were maintained in DMEM medium containing 10% FBS, 1% Penicillin/Streptomycin antibiotics.

For isolation of bone marrow-derived macrophages (BMDMs), mice were euthanized in a CO_2 chamber and death was confirmed by cervical dislocation. Bone marrow cells were harvested from the femur and the tibia and differentiated in DMEM (containing 10% fetal calf serum, 1% penicillin/streptomycin and 20% and 20 ng/mL M-CSF) for 6 days. 1×10^6 BMDMs per milliliter were used for LPS and/or OI treatments. Unless otherwise stated, the cells were pre-treated with OI (250 μM) for 12 hours and then stimulated with LPS (100 ng/ml). Moreover, the unmodified itaconic acid was adjusted to pH 7.0 with NaOH. Cells were pretreated with unmodified ITA for 12 hs using indicated dose.

For isolation of peritoneal macrophages, peritoneal exudate cells were elicited by intraperitoneal (i.p.) injection of 1 ml of Brewer's thioglycolate (Sigma) as previously described[52]. At 24 hours after i.p. injection, cells were harvested by peritoneal lavage using 5 ml of ice-cold, sterile PBS. Total cells were plated on a 90-mm dish and allowed to adhere for 24 hours. Cells were then washed 3 times with cold PBS to remove non-adherent cells, re-plated and treated with LPS (100 ng/ml) for indicated time.

Transfection and immunoprecipitation

Transfection of RAW264.7 cells was performed using Amaxa Cell Line Nucleofector Kit V according to the manufacturer's protocol (Lonza VCA-1003). For the other cell transfection, we used Lipofectamine 2000 (Invitrogen) or polyJet (SignaGen) following the manufacturer's instruction.

For immunoprecipitation, cells were washed with cold phosphate buffered saline (PBS) and lysed in NP-40 buffer, containing 50 mM Tris-HCl, 300 mM NaCl, 0.3% NP-40, pH 7.4 and protease inhibitor cocktail (Roche) with rotation at 4°C for 40 min. After centrifugation at 13000×g for 15 min at 4°C, the supernatant was incubated with indicated antibodies for 2 hrs, followed by incubation with Protein-A/G for another 1 hr at 4°C.

Histone methylation profiling by LC-MS/MS

Histone methylation was quantified by MRM-based LC-MS/MS method, as described by previous methods [53, 54]. In short, the core histones were acid extracted from tissue with 0.4 M H_2SO_4 and precipitated with trichloroacetic acid (TCA), followed by washing with ice-cold acetone twice. Then the histone protein was treated with N-Hydroxysuccinimide-propionate and digested with trypsin. Finally, the digested peptides were concentrated to dryness. Prior to the LC-MRM-MS, a mixture of isotope labeled histone peptides was added as internal standards to the samples, the histone peptides concentration in the samples was calculated by the peak area ratio of histone peptides to internal standard peptides.

Global DNA de/methylation quantification by LC-MS/MS

Genomic DNA from cultured cells was digested with DNA Degradase Plus (Zymo Research) at 37°C for 3 hrs. Deoxyguanosine (dG) was used as an internal control. The digested samples were then subjected to LC-MS/MS analysis using a ShimazuLC (LC-20AB pump) system coupled with 4000qtrap triple quadrupole mass spectrometer (AB sciex). A C18 column (250mm×2.1mm I.D., 3 μm particle size, ULTIMATE) was used. The mass spectrometer was optimized and set up in selected reaction monitoring (SRM) scan mode for monitoring the [M+H+] of 5mC (m/z 242.1→126.1), 5hmC (m/z 258.1142.1) and dG (m/z 268.1→ 152.1). The Analyst Software was used for analysis.

TET2 *in vitro* activity assay by dot-blot

In vitro assay of TET2 catalytic activity was performed using methylated dsDNA oligonucleotides as substrate. In brief, Flag-tagged mTET2^{CD} was ectopically expressed in Sf9 insect cells, immunoprecipitated, and eluted with Flag peptide. The reactions were carried out as described before[55], denatured and then neutralized. The reaction mixtures were spotted on nitrocellulose membrane, cross-linked and incubated overnight with antibodies recognizing 5mC (Active Motif, 2793764) or 5hmC (Active Motif, 10013602). Immunoblots were developed using secondary horseradish peroxidase (HRP)-coupled antibodies and a chemiluminescence kit.

TET2 *in vitro* activity assay by a commercial kit

The Epigenase™ 5mC-Hydroxylase TET Activity/Inhibition Assay Kit (P-3086-96) was used to determine TET2 enzyme activity, according to the manufacturer's protocol. In brief, 1 μL containing 120 ng of Flag-tagged mTET2^{CD} purified from Sf9 cells was added to a total reaction system of 50 μL, with or without metabolites. After a 30-min incubation at 37°C, absorbance at 450 nm was read.

TET2 *in vitro* activity assay using immobilized substrate DNA

TET2 *in vitro* activity assay was developed based on immobilized substrate DNA and fluorescence detection of 5hmC. Briefly, two complementary single-stranded and biotin-labelled oligonucleotides were synthesized at Sigma (5'GTATGCCTCATGC^{m}CGGACTTAACTGCAGTG 3', 3' CATACGGAGTACGG^{m}CCTGAATTGACGTCAC 5'-[Btn]. The superscript 'm' indicates the methylation of following cytosine, whereas 'Btn' means biotin label). 2 nmol of single-stranded oligonucleotides were mixed in annealing buffer (10 mM Tris, pH 8.0, 50 mM NaCl, 1 mM EDTA), boiled at 99 °C for 5 min and subsequently transferred to 90 °C-preheated water, which was gradually cooled down to room temperature. 50 pmol of annealed double-stranded DNA oligonucleotides were added to Pierce™ Streptavidin Coated High Capacity 96-wells plates (Catalog number: 15525) and immobilized at room temperature for 30 min. After substrate immobilization, reaction buffer (50 mM HEPES buffer (pH 8.0), 50 μM ammonium iron (II) sulfate, 0.1 mM α-KG, 2 mM ascorbic acid, 2.5 mM DTT, 100 mM NaCl, and 1.2 mM ATP[55]) with or without metabolites was added into each well, followed by addition of 120 ng of purified mTET2^{CD} per assay. The reactions were incubated at 37°C for 30 min with constant shaking on an Eppendorf ThermoMixer (700 r.p.m). 5hmC was detected by a first incubation with anti-5hmC antibody

for 3 hrs at room temperature, followed by 1-hr incubation at room temperature with a Fluorescent-dye conjugated secondary antibody or HRP conjugated secondary antibody. The amount of 5hmC was quantified by using a microreader with excitation at 495 nm and emission at 518 nm.

Nuclear magnetic resonance (NMR)

All samples were prepared in a buffer containing 20 mM BisTris (pH 6.5), 140 mM NaCl, 50 μM $FeSO_4$, 0.6 mM BME, and 80% D_2O, where ITA and α-KG stocks were first prepared at pH 6.5 with NaOH. Standard Bruker STD NMR measurements were carried out at 25^oC on a Bruker Avance III 700 MHz spectrometer equipped with a 5 mm triple-resonance cryogenic probe. With ^1H carrier being on water, a 3-second saturation was performed using a 50-millisecond EBurp2 pulse with a bandwidth of 0.75 ppm centered at 0.8 ppm or -40 ppm for difference and reference experiments, respectively. NMR data were processed using Bruker Topspin 3.5.7.

Gene deletion by CRISPR/Cas9 system

Tet2-KO and *Irg1*-KO RAW264.7 cells were generated through the CRISPR (clustered regularly interspaced short palindromic repeats)/Cas9 system[56]. Cells were transiently transfected with Cas9 and single-guide RNA (sgRNA) plasmid with EGFP expression (PX458; Addgene plasmid #48138). The gRNA sequences used for targeting *Tet2* and *Irg1* were AAAGTGCCAACAGATATCCA[31] and AGCTTTGCTGGTATGATTCA, respectively. Two days after transfection, single cells expressing EGFP were sorted into 96-well plates by using fluorescence-activated cell sorting (BD, FACSAria™ III). KO clones were validated by DNA sequencing and western-blot analysis.

Intracellular metabolite quantification by LC-MS/MS

Cell number and cell diameter were measured using and automated cell counter (Countstar). C_{13}-labelled ITA was added as internal standard. Cells were fixed by immediate addition of 1 ml 80% (v/v) chilled (-80°C) methanol. Cell extracts were analyzed by ultrahigh performance liquid chromatograph (Acquity UPLC I-Class, Waters) coupled to a Triple Quadrupole Mass Spectrometer (Xevo TQ-XS, Waters). Cells were assumed to have a spherical shape, and intracellular metabolite concentration was calculated using external standard curves and taking into account cellular diameter (d, micrometers) and cell number using the following equation: [metabolite] = metabolite quantity (moles)/((4/3000)π(d/2)3).

Immunofluorescence (IF)

Cells were washed with cold PBS, fixed with 4% PMSF (Sangon) for 15 min, and permeabilized with 0.3% Triton X-100 for 15 min at room temperature. For 5hmC staining, DNA was denatured with 2 N HCl for 30 min and then neutralized with 100 mM Tris-HCl (PH 8.5) for 10 min. After washing 3 times with PBS, samples were incubated with blocking buffer (3% BSA in PBS) for 1 hr, followed by incubation at 4°C overnight with anti-5hmC primary antibody. After washing 3 times with PBS, cells were incubated with Alexa Fluor 594 (Green) conjugated secondary antibody (Invitrogen) at room temperature for 1 hr. Cell

nucleus was stained with DAPI (Invitrogen). Images were captured using Leica fluorescence optical microscope.

Global 5hmC quantification by FACS

The FACS assay was performed as previously described[57]. Cells were re-suspended in FACS buffer (PBS with 1% BSA, 2 mM EDTA) and incubated with Fc blocker for 10 min on ice. After washing with FACS buffer, cells were fixed and permeabilized using the Cell Fixation/permeabilization kit (BD Biosciences). DNA was denatured by adding 2N HCl for 20 min and then neutralized with 10 mM Tris-HCl (pH 8.0) for 20 min. Anti-5hmC antibody (Active Motif, 1:200) and FITC conjugated goat anti-rabbit secondary antibody (1:200; Thermo Fisher Scientific) were used for 5hmC staining. Data were analyzed using the FlowJo software.

Global 5mC and 5hmC quantification by dot-blot

DNA dot-blot assay was performed as described previously with some modifications[19, 31, 58]. Briefly, genomic DNA was spotted on a nitrocellulose membrane (Whatman). The membrane was placed under an ultraviolet lamp for 20 min to crosslink DNA, and then blocked with 5% milk in TBS-Tween20 for 1 hr, followed by incubation with the anti-5mC or anti-5hmC antibody at 4°C overnight. After incubation with an HRP-conjugated secondary antibody (GeneScript) for 1 hr at RT, the membrane was washed with TBS-Tween 20 for three times and then scanned by a Typhoon scanner (GE Healthcare), and the quantification of 5mC or 5hmC was done by Image-Quanta software (GE Healthcare).

Hydroxymethylcytosine DNA immunoprecipitation sequencing (hMeDIP-seq)

5hmC mapping was conducted as described by previous methods[59]. Briefly, mouse BMDMs were pre-treated with or without 0.5 mM OI for 8 hrs, and then stimulated with 100 ng/ml LPS for 4 hrs. From these cells, 10 μg of sonicated and adaptor ligated genomic DNA was used as input, and 5 μL of 5hmC antibody (Active Motif) was used to immunoprecipitate modified DNA. Immunoprecipitated DNA was amplified for Illumina sequencing. Detailed DIP-Seq procedures as well as the following data analysis methods can be found in Extended Experimental Procedures. The DIP-seq datasets have been deposited in Gene Expression Omnibus (GEO) under the accession number GSE158580.

RNA purification and real-time quantitative PCR (qRT-PCR)

Total RNA was extracted from cells using TRIzol (Invitrogen) as recommended by the manufacturer's protocol. RNA was reversely transcribed using oligo-dT primers. Diluted cDNA was then used in qRT-PCR reactions containing SYBR Premix ExTaq (TaKaRa) and gene-specific primers. The reactions were performed in a QuantStudio™ 6 Flex Real-Time PCR System (Applied Biosystems). β-Actin was used as a housekeeping control. Primers were listed in extended Table 1.

RNA sequencing (RNA-seq)

RAW264.7 or BMDM cells were treated with or without LPS for 4 hrs and pre-treated with 250 μM OI for 12 hrs and then were subjected to RNA extraction. Each condition was prepared in triplicate for each RNA-seq experiment. Library preparation was done using the Illumina TrueSeq mRNA sample preparation kit and sequencing on Illumina HiSeq4000 machine was performed by High Throughput Genomic Sequencing in Novagene. Paired-end FASTQ sequences were aligned to the mouse genome (mm10). Differential gene expression analysis was performed using the DESeq2 package and selecting raw gene counts output from Rsubread[60]. Datasets have been deposited in Gene Expression Omnibus (GEO) under the accession number GSE148143, GSE148145 and GSE148147.

Chromatin-immunoprecipitation with quantitative PCR (ChIP-qPCR)

ChIP assay was performed as described previously[61]. Briefly, cells were cross-linked with 1% paraformaldehyde and sonicated at 4°C for 20 min (Bioruptor, low mode). Chromatin was immunoprecipitated at 4°C for 3 hrs with indicated antibodies. Antibody-chromatin complexes were pulled-down using protein A-Sepharose (RepliGen), washed and eluted. After cross-link reversal and proteinase K (TaKaRa) treatment, immunoprecipitated DNA was extracted using a PCR Purification Kit (QIAGEN). The DNA fragments were further analyzed by real-time quantitative PCR using the primers as listed in extended Table 1.

Hydroxymethylated DNA immunoprecipitation with quantitative PCR, hMeDIP-qPCR

The hMeDIP-qPCR assay was performed as previously described[62]. Briefly, 2 μg genomic DNA was extracted from cultured cells by the phenol-chloroform method and then denatured and immunoprecipitated with anti-5hmC (Active Motif) or rabbit IgG antibody (Millipore) and protein G-sepharose (Invitrogen). Beads were washed for three times and treated with proteinase K for 4 hrs. DNA was extracted using a PCR Purification Kit (QIAGEN) and analyzed by real-time quantitative PCR using the primers as listed in Extended table 1.

Mouse models of LPS-induced sepsis

Mice (8-10 weeks of age) were intraperitoneally injected with 50 mg/kg ITA (pH=7.0) for 12 hrs, prior to LPS challenge whenever indicated. Blood and tissue samples were harvested at indicated times. Whole-blood samples were allowed to coagulate for 15 minutes at room temperature and centrifuged at 4,000×rpm for 5 min to collect serum. Serum levels of Il-6 (Cat. No. 70-EK206/3-96), Il-1β (Cat. No. 70-EK201B/3-96) and Cxcl9 (Cat. No. 70-EK2143/2-96) were determined by using ELISA Kits (Multi Sciences). Serum Tnf-α (Cat. No. E-EL-M0049c) was determined by using a ELISA kit from Elabscience.

To quantify the magnitude of liver injury induced by LPS, serum activities of alanine transaminase (ALT) and aspartate transaminase (AST) were measured using commercial kits (Nanjing Jiancheng). To quantify the magnitude of pulmonary edema induced by LPS, whole-lung tissue of each individual mouse was collected, rinsed to remove surface blood, and patted dry, and the immediate weight was recorded as the wet weight. The tissue was air dried for 1 day and the weight was recorded as the dry weight for

calculating the lung wet/dry weight ratio. Furthermore, lung histopathological injury was assessed by hematoxylin and eosin (HE) staining, and acute lung injury was scored as follows: a) alveolar congestion, b) hemorrhage, c) infiltration or aggregation of neutrophils in airspace or vessel wall, and d) thickness of alveolar wall/hyaline membrane formation. Each item was scored on a 5-point scale as follows: 0 = minimal damage, 1+ = mild damage, 2+ = moderate damage, 3+ = severe damage, and 4+ = maximal damage[63]. For the survival assay, animals were carefully monitored as previously reported[8]. Humane end point for the experiment was based on body condition, physical condition and unprovoked behavior.

Statistical analysis

Statistical analyses were performed with two-tailed Student's t-test for paired comparisons or two-way ANOVA for multiple comparisons followed by Bonferroni post-tests. Data shown (if not pointed out) represents the results obtained from triplicate independent experiments with mean +/- Standard Deviation (S.D.) or standard error of the mean (SEM). The values of $p < 0.05$ were considered statistically significant.

Declarations

Author contributions

Y. X., K-L. G. and D. Y. conceived and supervised the project; L-L. C. designed the experiments and performed most of the experiments with Z-L C. L-L.C. wrote the draft with Y.X and D. Y.; C. M. participated in the initiation the project. A. J. and Q. Z. performed NMR studies using the TET2 protein provided by Z-Z R; C. M., C. Z., J-Y. Z., Y-Y. L, measured the intracellular levels of ITA and other metabolites; X-F. C. and C. M. performed immunofluorescence staining for 5hmC in HEK293T cells and generated constructs overexpressing Irg1 and catalytic defect mutant; J-B. S generated *Irg1*-KO RAW264.7 cells; M. S., Y-Z. Z. and C. M. performed 5hmC DIP-Seq under the supervision of L. S.; H. Y. and L. Y. performed 5hmC staining; Z-L C. and Z-J. L. quantified genomic 5hmC and 5mC in cells by dot-blot and LC-MS/MS, respectively; C-X. H. performed *in vitro* assay for KDM activity under the supervision of F. L. (data not shown); Y-J. G., K-Y. L., C.M., G-P. L., and T.Q. conducted LPS administration in mice under the supervision of Y-F. Z. and X. C.; N. Z. performed mouse BMT under the supervision of C-W. D.; Y-P. X. made initial finding of NF-κB and TET2 interaction; A. S. B. participated in the design of NF-κB related experiments; X-M. T. performed statistical analyses.

Acknowledgements

We thank Joshua Boyer, Stu Parnham and UNC Biomolecular NMR Spectroscopy Core Facility for the NMR analysis, Matt Lee of Molecular Cornerstones for molecular modeling, Yanhui Xu (Fudan University) for providing human $TET2^{CD}$ expression vector, Jiemin Wong (East China Normal University) for providing human TET3 expression vector, and Nick Brown (UNC-Chapel Hill) for advising TET2 purification, and Jiayu Chen and Shaorong Gao (School of Life Sciences and Technology, Tongji University, Shanghai) for providing *Tet2*^{HxD} KI mutant mice. We also thank the staff members working at IBS, Fudan University for their help on mass spectrometry analyses. This work was supported by National Key R&D Program of

China (2016YFA0501800 and 2020YFA0803202 to D. Y.; 2016YFC1305102 to Y.Z.), the NSFC grants (No. 31871431, No. 31821002 to D. Y; No. 81671561, No. 81974248 to Y. Z.), the Innovative research team of high-level local universities in Shanghai (to D. Y.), and Program for Outstanding Medical Academic Leader (2019LJ19 to Y.Z.). This study was also supported by Samuel Waxman Research Foundation Investigator Award and NIH grant CA163834 (A. S. B. and Y. X).

References

1. Daniels, B.P. *et al.* The Nucleotide Sensor ZBP1 and Kinase RIPK3 Induce the Enzyme IRG1 to Promote an Antiviral Metabolic State in Neurons. *Immunity* **50**, 64-76 e64 (2019).

2. Nair, S. *et al.* Irg1 expression in myeloid cells prevents immunopathology during M. tuberculosis infection. *J Exp Med* **215**, 1035-1045 (2018).

3. Lee, C.G., Jenkins, N.A., Gilbert, D.J., Copeland, N.G. & O'Brien, W.E. Cloning and analysis of gene regulation of a novel LPS-inducible cDNA. *Immunogenetics* **41**, 263-270 (1995).

4. Michelucci, A. *et al.* Immune-responsive gene 1 protein links metabolism to immunity by catalyzing itaconic acid production. *Proc Natl Acad Sci U S A* **110**, 7820-7825 (2013).

5. Ackermann, W.W. & Potter, V.R. Enzyme inhibition in relation to chemotherapy. *Proc Soc Exp Biol Med* **72**, 1-9 (1949).

6. Lampropoulou, V. *et al.* Itaconate Links Inhibition of Succinate Dehydrogenase with Macrophage Metabolic Remodeling and Regulation of Inflammation. *Cell Metab* **24**, 158-166 (2016).

7. Cordes, T. *et al.* Immunoresponsive Gene 1 and Itaconate Inhibit Succinate Dehydrogenase to Modulate Intracellular Succinate Levels. *J Biol Chem* **291**, 14274-14284 (2016).

8. Mills, E.L. *et al.* Itaconate is an anti-inflammatory metabolite that activates Nrf2 via alkylation of KEAP1. *Nature* **556**, 113-117 (2018).

9. Bambouskova, M. *et al.* Electrophilic properties of itaconate and derivatives regulate the IkappaBzeta-ATF3 inflammatory axis. *Nature* **556**, 501-504 (2018).

10. Qin, W. *et al.* S-glycosylation-based cysteine profiling reveals regulation of glycolysis by itaconate. *Nature chemical biology* **15**, 983-991 (2019).

11. Hu, L. *et al.* Crystal structure of TET2-DNA complex: insight into TET-mediated 5mC oxidation. *Cell* **155**, 1545-1555 (2013).

12. Chowdhury, R. *et al.* The oncometabolite 2-hydroxyglutarate inhibits histone lysine demethylases. *EMBO Rep* **12**, 463-469 (2011).

13. Xu, W. *et al.* Oncometabolite 2-hydroxyglutarate is a competitive inhibitor of alpha-ketoglutarate-dependent dioxygenases. *Cancer cell* **19**, 17-30 (2011).

14. Seim, G.L. *et al.* Two-stage metabolic remodelling in macrophages in response to lipopolysaccharide and interferon-gamma stimulation. *Nature metabolism* **1**, 731-742 (2019).

15. Liu, P.S. *et al.* alpha-ketoglutarate orchestrates macrophage activation through metabolic and epigenetic reprogramming. *Nature immunology* **18**, 985-994 (2017).

16. Xiao, M. *et al.* Inhibition of alpha-KG-dependent histone and DNA demethylases by fumarate and succinate that are accumulated in mutations of FH and SDH tumor suppressors. *Genes Dev* **26**, 1326-1338 (2012).

17. O'Neill, L.A.J. & Artyomov, M.N. Itaconate: the poster child of metabolic reprogramming in macrophage function. *Nat Rev Immunol* **19**, 273-281 (2019).

18. Zhang, Q. *et al.* Tet2 is required to resolve inflammation by recruiting Hdac2 to specifically repress IL-6. *Nature* **525**, 389-393 (2015).

19. Wang, Y. *et al.* WT1 recruits TET2 to regulate its target gene expression and suppress leukemia cell proliferation. *Molecular cell* **57**, 662-673 (2015).

20. Yamamoto, M. *et al.* Regulation of Toll/IL-1-receptor-mediated gene expression by the inducible nuclear protein IkappaBzeta. *Nature* **430**, 218-222 (2004).

21. Miyake, T. *et al.* IkappaBzeta is essential for natural killer cell activation in response to IL-12 and IL-18. *Proc Natl Acad Sci U S A* **107**, 17680-17685 (2010).

22. Okamoto, K. *et al.* IkappaBzeta regulates T(H)17 development by cooperating with ROR nuclear receptors. *Nature* **464**, 1381-1385 (2010).

23. Johansen, C. *et al.* IkappaBzeta is a key driver in the development of psoriasis. *Proc Natl Acad Sci U S A* **112**, E5825-5833 (2015).

24. Alexander, E. *et al.* IkappaBzeta is a regulator of the senescence-associated secretory phenotype in DNA damage- and oncogene-induced senescence. *J Cell Sci* **126**, 3738-3745 (2013).

25. Xu, H. *et al.* Chronic inflammation in fat plays a crucial role in the development of obesity-related insulin resistance. *J Clin Invest* **112**, 1821-1830 (2003).

26. Nagarsheth, N., Wicha, M.S. & Zou, W. Chemokines in the cancer microenvironment and their relevance in cancer immunotherapy. *Nat Rev Immunol* **17**, 559-572 (2017).

27. Liu, T., Zhang, L., Joo, D. & Sun, S.C. NF-kappaB signaling in inflammation. *Signal transduction and targeted therapy* **2** (2017).

28. Rampal, R. *et al.* DNA hydroxymethylation profiling reveals that WT1 mutations result in loss of TET2 function in acute myeloid leukemia. *Cell Rep* **9**, 1841-1855 (2014).

29. Ichiyama, K. *et al.* The methylcytosine dioxygenase Tet2 promotes DNA demethylation and activation of cytokine gene expression in T cells. *Immunity* **42**, 613-626 (2015).

30. Ma, S. *et al.* Epigenetic regulator CXXC5 recruits DNA demethylase Tet2 to regulate TLR7/9-elicited IFN response in pDCs. *J Exp Med* **214**, 1471-1491 (2017).

31. Xu, Y.P. *et al.* Tumor suppressor TET2 promotes cancer immunity and immunotherapy efficacy. *J Clin Invest* **130**, 4316-4331 (2019).

32. Yamazaki, S., Muta, T., Matsuo, S. & Takeshige, K. Stimulus-specific induction of a novel nuclear factor-kappaB regulator, IkappaB-zeta, via Toll/Interleukin-1 receptor is mediated by mRNA stabilization. *J Biol Chem* **280**, 1678-1687 (2005).

33. Link, V.M. *et al.* Analysis of Genetically Diverse Macrophages Reveals Local and Domain-wide Mechanisms that Control Transcription Factor Binding and Function. *Cell* **173**, 1796-1809 e1717 (2018).

34. Zhao, Z. *et al.* The catalytic activity of TET2 is essential for its myeloid malignancy-suppressive function in hematopoietic stem/progenitor cells. *Leukemia* **30**, 1784-1788 (2016).

35. Ye, D., Guan, K.L. & Xiong, Y. Metabolism, Activity, and Targeting of D- and L-2-Hydroxyglutarates. *Trends Cancer* **4**, 151-165 (2018).

36. Ryan, D.G. *et al.* Coupling Krebs cycle metabolites to signalling in immunity and cancer. *Nature metabolism* **1**, 16-33 (2019).

37. Arts, R.J. *et al.* Glutaminolysis and Fumarate Accumulation Integrate Immunometabolic and Epigenetic Programs in Trained Immunity. *Cell Metab* **24**, 807-819 (2016).

38. Lio, C.J., Yuita, H. & Rao, A. Dysregulation of the TET family of epigenetic regulators in lymphoid and myeloid malignancies. *Blood* **134**, 1487-1497 (2019).

39. Jaiswal, S. & Libby, P. Clonal haematopoiesis: connecting ageing and inflammation in cardiovascular disease. *Nat Rev Cardiol* **17**, 137-144 (2020).

40. Cook, E.K., Luo, M. & Rauh, M.J. Clonal hematopoiesis and inflammation: Partners in leukemogenesis and comorbidity. *Exp Hematol* **83**, 85-94 (2020).

41. Chen, M. *et al.* Itaconate is an effector of a Rab GTPase cell-autonomous host defense pathway against Salmonella. *Science* **369**, 450-455 (2020).

42. Basler, T., Jeckstadt, S., Valentin-Weigand, P. & Goethe, R. Mycobacterium paratuberculosis, Mycobacterium smegmatis, and lipopolysaccharide induce different transcriptional and post-

transcriptional regulation of the IRG1 gene in murine macrophages. *J Leukoc Biol* **79**, 628-638 (2006).

43. Preusse, M., Tantawy, M.A., Klawonn, F., Schughart, K. & Pessler, F. Infection- and procedure-dependent effects on pulmonary gene expression in the early phase of influenza A virus infection in mice. *BMC Microbiol* **13**, 293 (2013).

44. Cho, H. *et al.* Differential innate immune response programs in neuronal subtypes determine susceptibility to infection in the brain by positive-stranded RNA viruses. *Nat Med* **19**, 458-464 (2013).

45. Smith, J. *et al.* Systems analysis of immune responses in Marek's disease virus-infected chickens identifies a gene involved in susceptibility and highlights a possible novel pathogenicity mechanism. *J Virol* **85**, 11146-11158 (2011).

46. Safronova, A. *et al.* Alarmin S100A11 initiates a chemokine response to the human pathogen Toxoplasma gondii. *Nat Immunol* **20**, 64-72 (2019).

47. Li, Y. *et al.* Immune responsive gene 1 (IRG1) promotes endotoxin tolerance by increasing A20 expression in macrophages through reactive oxygen species. *J Biol Chem* **288**, 16225-16234 (2013).

48. Hall, C.J. *et al.* Epidermal cells help coordinate leukocyte migration during inflammation through fatty acid-fuelled matrix metalloproteinase production. *Nat Commun* **5**, 3880 (2014).

49. Sun, K.A. *et al.* Endogenous itaconate is not required for particulate matter-induced NRF2 expression or inflammatory response. *Elife* **9** (2020).

50. Weiss, J.M. *et al.* Itaconic acid mediates crosstalk between macrophage metabolism and peritoneal tumors. *J Clin Invest* **128**, 3794-3805 (2018).

51. Cheon, Y.P., Xu, X., Bagchi, M.K. & Bagchi, I.C. Immune-responsive gene 1 is a novel target of progesterone receptor and plays a critical role during implantation in the mouse. *Endocrinology* **144**, 5623-5630 (2003).

52. Zhang, X., Goncalves, R. & Mosser, D.M. The isolation and characterization of murine macrophages. *Current protocols in immunology* **Chapter 14**, Unit 14 11 (2008).

53. Gao, J. *et al.* Absolute quantification of histone PTM marks by MRM-based LC-MS/MS. *Anal Chem* **86**, 9679-9686 (2014).

54. Yu, Y. *et al.* Quantitative Profiling of Combinational K27/K36 Modifications on Histone H3 Variants in Mouse Organs. *J Proteome Res* **15**, 1070-1079 (2016).

55. Nakagawa, T. *et al.* CRL4(VprBP) E3 ligase promotes monoubiquitylation and chromatin binding of TET dioxygenases. *Molecular cell* **57**, 247-260 (2015).

56. Ran, F.A. *et al.* Genome engineering using the CRISPR-Cas9 system. *Nat Protoc* **8**, 2281-2308 (2013).

57. Lee, M., Zhou, Y. & Huang, Y. An Engineered Split-TET2 Enzyme for Chemical-inducible DNA Hydroxymethylation and Epigenetic Remodeling. *J Vis Exp* (2017).

58. Lv, L. *et al.* Vpr Targets TET2 for Degradation by CRL4(VprBP) E3 Ligase to Sustain IL-6 Expression and Enhance HIV-1 Replication. *Molecular cell* **70**, 961-970 e965 (2018).

59. Shen, L. *et al.* Genome-wide analysis reveals TET- and TDG-dependent 5-methylcytosine oxidation dynamics. *Cell* **153**, 692-706 (2013).

60. Liao, Y., Smyth, G.K. & Shi, W. The R package Rsubread is easier, faster, cheaper and better for alignment and quantification of RNA sequencing reads. *Nucleic acids research* **47**, e47 (2019).

61. Chen, L.L. *et al.* SNIP1 Recruits TET2 to Regulate c-MYC Target Genes and Cellular DNA Damage Response. *Cell Rep* **25**, 1485-1500 e1484 (2018).

62. Lan, F. *et al.* Recognition of unmethylated histone H3 lysine 4 links BHC80 to LSD1-mediated gene repression. *Nature* **448**, 718-722 (2007).

63. Mikawa, K., Nishina, K., Takao, Y. & Obara, H. ONO-1714, a nitric oxide synthase inhibitor, attenuates endotoxin-induced acute lung injury in rabbits. *Anesthesia and analgesia* **97**, 1751-1755 (2003).

Figures

Figure 1. Itaconate binds directly to TET2 in a manner similar to α-KG

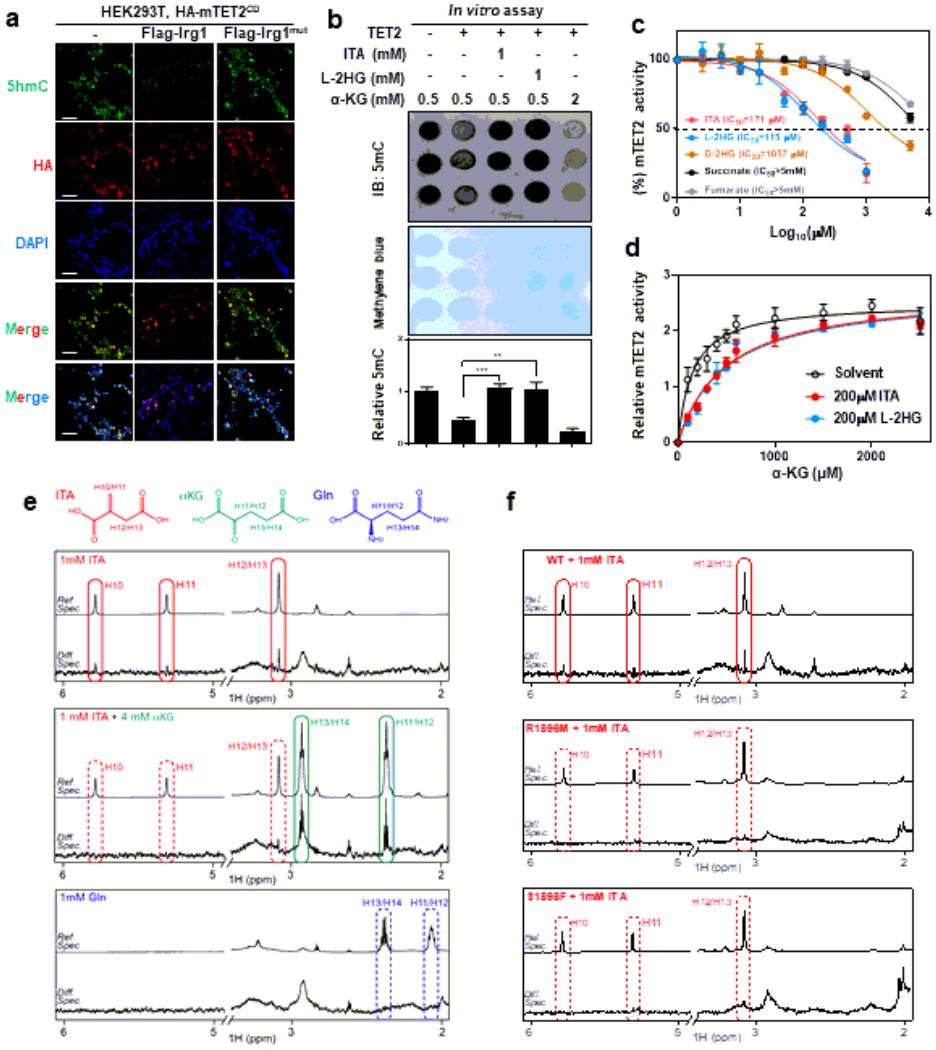

Figure 1

Itaconate binds directly to TET2 in a manner similar to α-KG a, Overexpression of Irg1, but not Irg1mut, inhibits Tet2 activity in cells. Flag-tagged wild-type Irg1 or catalytic defect mutant was co-expressed with HA-mTET2CD in HEK293T cells and was then subjected to detect 5hmC by immunofluorescence staining using indicated antibodies. Scale bar, 50 μM. b, ITA competitively inhibits α-KG-dependent Tet2 activity. Tet2 activity was measured in vitro by 5mC dot-blot assays using mTET2CD purified from Sf9 insect cells

and methylated dsDNA oligonucleotides as substrate in the presence of indicated metabolites. Shown are average values with S.D. of triplicate experiments. P- values are calculated using two-tailed Student's t-test. ***denotes $p < 0.001$ for the indicated comparison. c, IC50 values of indicated metabolites toward mTET2CD were measured by a protocol modified from the method shown in Extended Data Fig. 2c. Enzyme activity was analyzed using GraphPad software and IC50 values were calculated using the equation of log (inhibitor) vs. response (three parameters). Shown are average values with standard deviation (S.D.) of triplicate experiments. d, α-KG overcomes ITA and L-2HG inhibition of Tet2. The relative Tet2 enzyme activity was measured as in Fig. 1c in the presence of fixed concentration of ITA or L-2-HG and variable concentration of α-KG. Data was analyzed using GraphPad software following Michaelis-Menten equation. Shown are average values with S.D. of triplicate experiments. e, ITA binds to TET2 and is competed off by α-KG. Saturation transfer difference (STD) NMR spectroscopy was used to determine the binding of metabolites with recombinant human TET2CD as previously described11. Chemical structures of metabolites are shown on top. Each panel below includes standard 1H NMR spectrum (Ref.) and STD 1H NMR spectrum (Diff.) for indicated metabolite in the presence of TET2 (10 μM). Highlighted in red are observable 1H NMR signals of ITA (1 mM), where STD signals indicate binding of ITA to TET2. Highlighted in red and green are observable 1H NMR signals of ITA and α-KG (4 mM), respectively. Binding of α-KG to TET2, as evidenced with α-KG STD signals, outcompetes binding of ITA to TET2 as seen by the disappearance or reduction of ITA STD signals. Gln (1 mM, blue) does not bind to TET and was included as a negative control. f, ITA is unable to bind with TET2 mutants. STD NMR spectroscopy was used to determine the binding of ITA with recombinant proteins of TET2CD mutant, i.e. R1896M or S1898F. Shown are average values with S.D. of triplicate experiments. P values are calculated using two-tailed Student's t-test for paired comparisons. **denotes $p < 0.01$, ***denotes $p < 0.001$ for the indicated comparison.

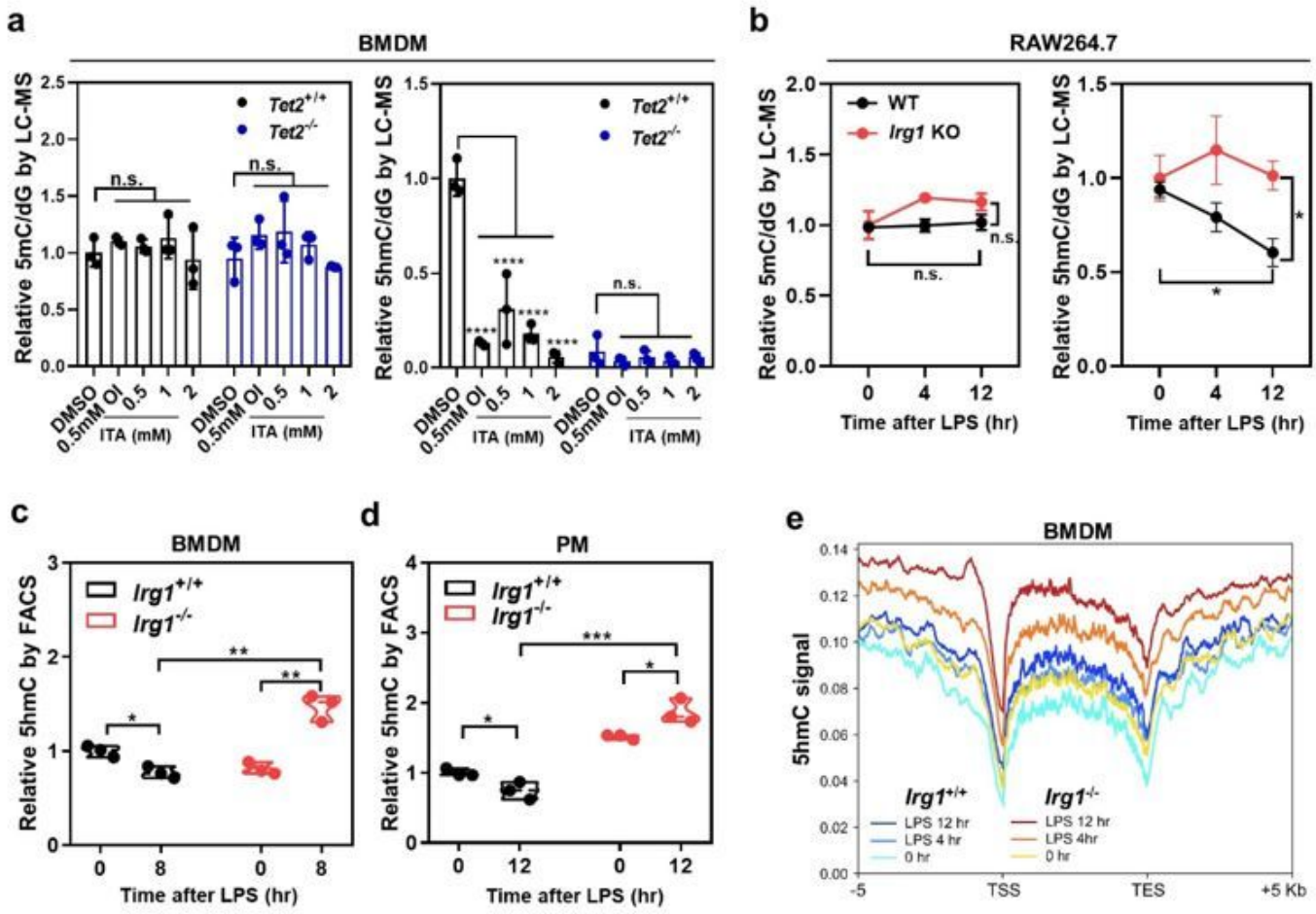

Figure 2

Irg1 produces Itaconate to inhibit Tet activity in vivo a, Treatment with OI or unmodified ITA reduces genome-wide 5hmC in Tet2+/+ BMDMs, but not Tet2-/- cells. Mouse BMDMs were treated with 0.5 mM OI or increased concentrations of unmodified ITA as indicated for 8 hours. Global levels of 5mC and 5hmC were quantified by LC-MS/MS. b, LPS treatment reduces genome-wide 5hmC in Irg1-WT but not Irg1-KO RAW264.7 cells. Macrophages were treated with LPS for indicated time, and global levels of 5mC and 5hmC were determined by LC-MS/MS. c, d, LPS treatment reduces genome-wide 5hmC in Irg1+/+ but not Irg1-/- primary macrophages. Mouse BMDMs (c) and peritoneal macrophage (d) were isolated and then treated with LPS for indicated time. Genomic 5hmC was determined by FACS. e, Deletion of Irg1 leads to increased 5hmC at promoters and intragenic regions. Irg1+/+ and Irg1-/- BMDMs were treated with LPS for indicated time, following 5hmC mapping by hMeDIP-seq. The normalized density profile for 5hmC across gene body + 5kb flanking regions is shown. Shown are average values with S.D. or SEM. of triplicate experiments. P values are calculated using two-tailed Student's t-test for paired comparisons or two-way ANOVA for multiple comparisons.*denotes $p < 0.05$, **denotes $p < 0.01$, ***denotes $p < 0.001$, and ****denotes $p < 0.0001$ for the indicated comparison. n.s. = not significant.

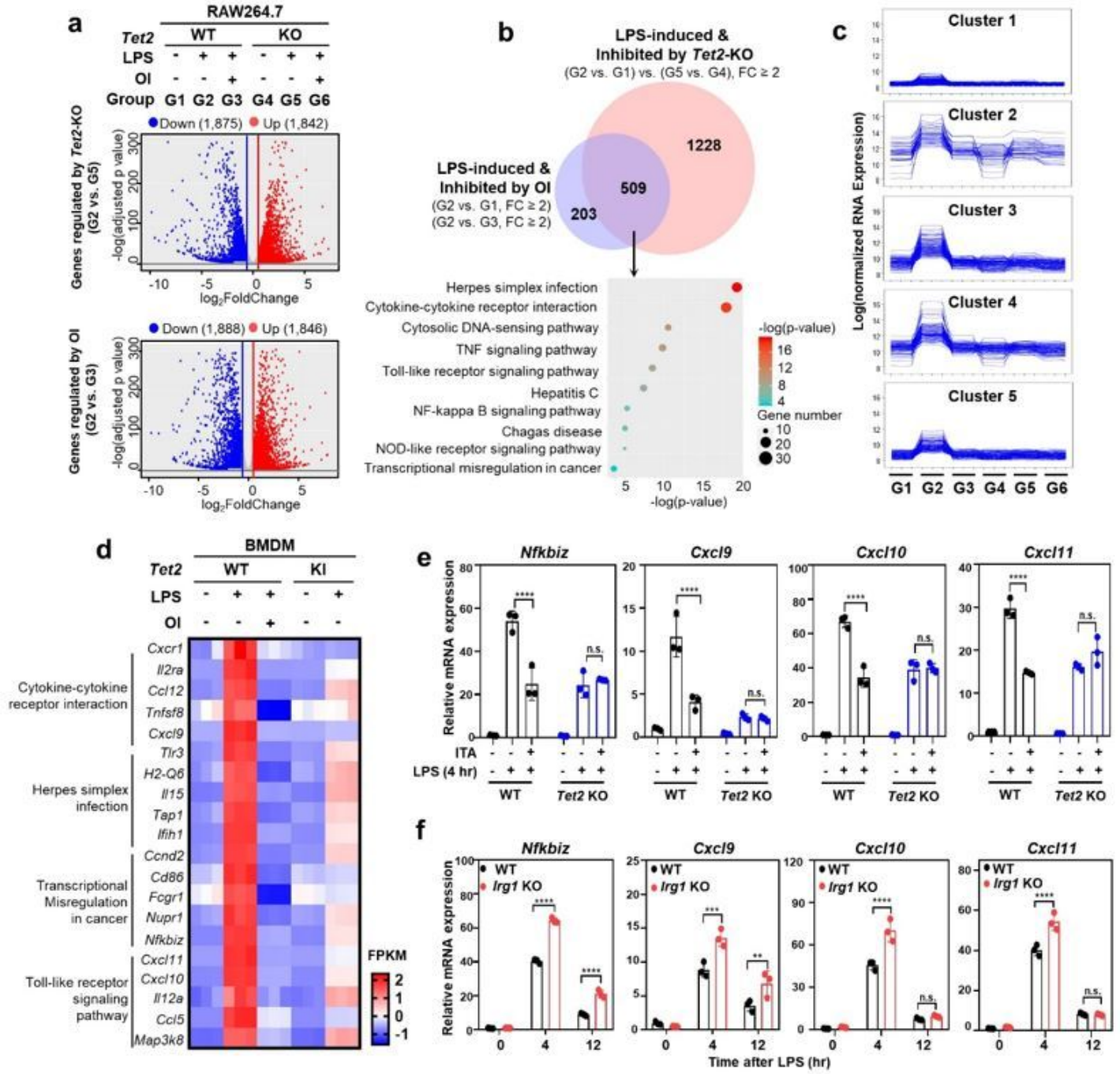

Figure 3

Tet2 is a major target of Itaconate to suppress LPS-induced genes in macrophages a, Volcano representation of RNA-seq analyses of the effect of OI treatment and Tet2 deletion on regulating gene expression in LPS-treated RAW264.7 cells. All genes differentially expressed with p-value ≤ 0.05 and fold change (FC) ≥2 are highlighted in red (up-regulation) and blue (down-regulation). b, Overlap between LPS-induced genes down-regulated by OI and by Tet2 deletion in RAW264.7 cells is displayed by Venn diagram (p-value < 10−10). Top 10 pathways enriched among the overlapping genes were identified by KEGG pathway analysis. c, K-mean cluster analysis of 712 which are induced by LPS and down-regulated

by OI in RAW264.7 cells, see also Extended Data Fig. 9c. d, Representative LPS-induced genes inhibited by OI and Tet2 catalytic inactivation in BMDMs. Top LPS-induced genes most significantly affected by OI in BMDMs are selected from 4 signaling pathways that are also affected by OI and Tet2-KO in RAW264.7 macrophages. e, Unmodified ITA inhibits LPS-induced genes in a Tet2-dependent manner. Tet2-WT and Tet2-KO RAW264.7 cells were pre-treated with unmodified ITA (3 mM) and then stimulated with LPS, following detection of the indicated gene mRNA expression by qRT-PCR. f, Deletion of Irg1 leads to up-regulation of genes which are induced by LPS but inhibited by either ITA or Tet2 catalytic inactivation. Irg1-WT and Irg1-KO RAW264.7 cells were treated with LPS for indicated time, following determination of indicated gene mRNA expression by qRT-PCR. Shown are average values with S.D. of triplicate experiments. P values are calculated using two-tailed Student's t-test for paired comparisons or two-way ANOVA for multiple comparisons. **denotes $p < 0.01$, ***denotes $p < 0.001$, and ****denotes $p < 0.0001$ for the indicated comparison. n.s. = not significant.

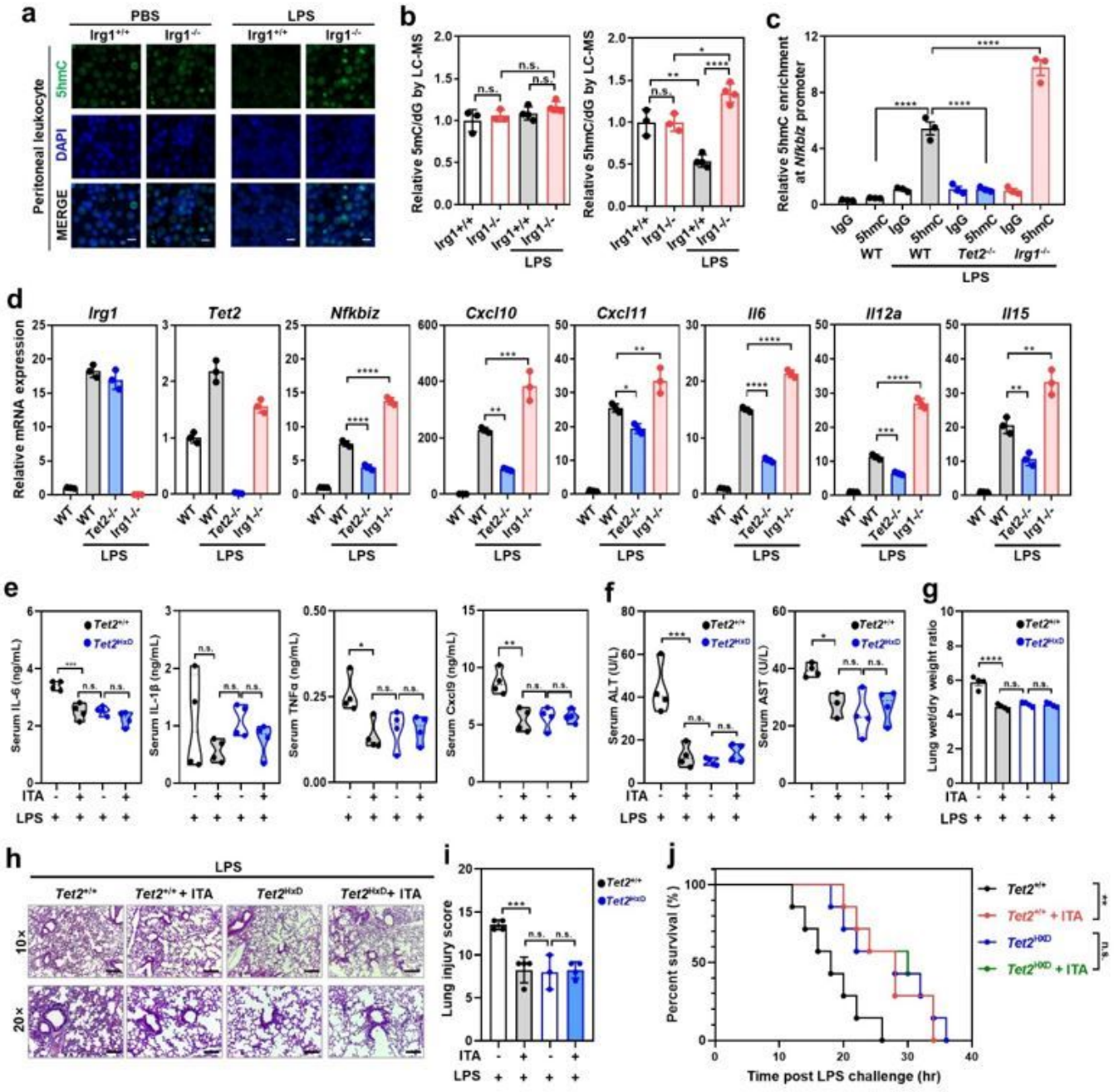

Figure 4

Itaconate reduces LPS-induced mouse mortality in a manner dependent on Tet2 a,b, Deletion of Irg1 leads to higher levels of genomic 5hmC in vivo. Peritoneal leukocytes were freshly isolated from indicated mice at 4 hours post i.p. injection of PBS or LPS (20 mg/kg). Genomic 5hmC was detected by immunofluorescence staining (IF, n=3 per group) (a) and LC-MS/MS (n=3-4 per group) (b). Representative IF result is shown. Scale bar, 20 μm. c, Deletion of Tet2 and Irg1 leads to decreased and increased levels of 5hmC at the promoter of Nfkbiz, respectively. As described above in (a-b), peritoneal leukocytes were harvested from Tet2-/-, Irg1-/-, and corresponding WT animals after i. p. LPS injection. In these cells, the Nfkbiz promoter enrichment of 5hmC was determined by hMeDIP-qPCR. d, Deletion of Tet2 and Irg1 leads

to down-regulation and up-regulation of genes, respectively, which are induced by LPS but inhibited by either ITA or Tet2 catalytic inactivation. As described above in (a-b), mouse peritoneal leukocytes were harvested and analyzed for indicated gene expression by qRT-PCR. e, ITA attenuates LPS-induced increases in pro-inflammatory cytokines and chemokines in WT, but not Tet2HxD chimeric mice. Briefly, transplanted mice were i.p. injected with ITA prior to LPS challenge (25 mg/kg; n=4 per group). At 4 hours post LPS, serum levels of indicated cytokines /chemokines were determined as described in Methods. f, ITA attenuates LPS-induced liver damage in WT, but not Tet2HxD chimeric mice. As described above in (e), serum samples were collected for measurement of ALT and AST activities as described in Methods. g,h,i, ITA attenuates LPS-induced pulmonary edema and lung injury in WT, but not Tet2HxD chimeric mice. As described above in (e), lung tissues of transplanted mice(n=3-4) were harvested and then subjected to the wet/dry weight ratio calculation (g) as well as HE staining (h). The injury score was determined as described in Methods (i). Representative photomicrographs are shown. Scale bar, 200 μm (upper panels)& 100 μm (lower panels). j, ITA protects LPS-induced lethality in WT, but not Tet2HxD chimeric mice. Briefly, transplanted mice were i.p. injected with ITA prior to LPS challenge (25 mg/kg; n=7 per group), and the animal survival was monitored and Kaplan-Meier survival curves were determined as described in Methods. Shown are average values with S.D. or SEM. of triplicate experiments (if not pointed out). P- values are calculated using two-tailed Student's t-test for paired comparisons or two-way ANOVA for multiple comparisons; As for the percent survival, P values were determined using log-rank (Mantel-Cox) test comparing each 2 groups; *denotes $p < 0.05$, **denotes $p < 0.01$, ***denotes $p < 0.001$, and ****denotes $p < 0.0001$ for the indicated comparison. n.s. = not significant.

Supplementary Files

This is a list of supplementary files associated with this preprint. Click to download.

- ExtendedDataFigures.docx